



XUNTA DE GALICIA

CONSELLERÍA DE EDUCACIÓN, UNIVERSIDADE
E FORMACIÓN PROFESIONAL



CAMPUS
TERRA



Agrupación Estratégica de Investigación del
Campus Terra de la USC **Biorrecursos:
Desarrollo y Producción Sostenible ‘BioReDes’**

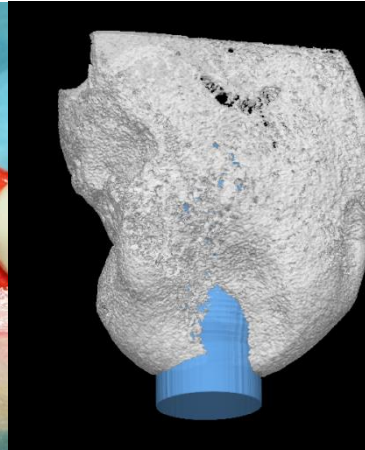
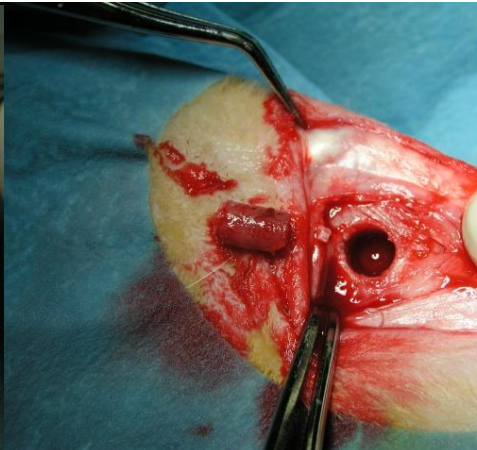
**Grupo de investigación:
CIRUGÍA EXPERIMENTAL G1708
“CIRUGIA, RADIOLOGIA Y
ECOGRAFIA VETERINARIA”**

CIRUGÍA EXPERIMENTAL G1708

González Cantalapiedra, Antonio
Barreiro Lois, Andrés
Barreiro Vázquez, José Daniel
López García, Mariano
López Peña, Mónica
Miño Fariña, Natalia
Muñoz Guzón, Fernando María
Varela López, Óscar
Vila Pastor, Mónica
Villanueva Santamarina, Blanca Lidia
Fernández Martín, Silvia
González Rellán, Sonia
Permuy Mendaña, María
Valiño Cultelli, Maria Victoria

CIRUGÍA EXPERIMENTAL G1708

Diagnóstico por Imagen
Realización de Pruebas “in vivo”
Laboratorio Investigación
Actividad Asistencial



✓ Actividad clínica del servicio de DPI

Fauna marina

Fondos marinos (geología sedimentaria)

Acuicultura

Journal of Veterinary Diagnostic Investigation

<http://jvdi.sagepub.com/>

Localized Pleural Mesothelioma Causing Cranial Vena Cava Syndrome in a Dog
Luciano Espino, Sonia Vazquez, Daniel Falde, Andres Barreiro, Natalia Miño and Ana Goicoa

J Vet Diagn Invest 2010; 22: 309
DOI: 10.1177/1043986210362002

The online version of this article can be found at
<http://jvdi.sagepub.com/content/22/2/309>

Published by:

 SAGE
<http://www.sagepub.com>

On behalf of:



Official Publication of the American Association of Veterinary Laboratory Diagnosticians, Inc.

J Vet Diagn Invest 22(309-312) (2010)

Localized pleural mesothelioma causing cranial vena cava syndrome in a dog

Luciano Espino,¹ Sonia Vazquez, Daniel Falde, Andres Barreiro, Natalia Miño, Ana Goicoa

Abstract. A 9-year-old female crossbred dog was presented to the Hospital Universitario Veterinario Ref Codina (Universidad de Santiago de Compostela, Lugo, Spain) for acute onset of severe, progressive swelling of the head, neck, and cranial/trunk. Survey radiographs and ultrasonography revealed a large, heterogeneous mass in the cranial mediastinum, compressing or growing into a large blood vessel within the cranial mediastinum and displacing the heart dorsocaudally. At postmortem examination, the mass was diagnosed as a large, localized mesothelioma. Localized mesotheliomas are rare neoplasms in dogs but should be considered as a possible differential diagnosis for cranial vena cava syndrome. The anatomic distribution and clinical features of mesothelioma in the present report are similar to other cases in humans.

Key words: Dogs; mediastinal neoplasia; mesothelioma; vena cava syndrome.

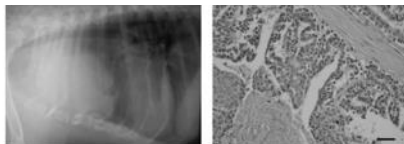


Figure 1. Right lateral thoracic radiograph (A) with defined cranial thoracic mass, approximately 4 cm in diameter is present. The heart is displaced dorsocaudally by the mass.

Figure 2. Light micrograph, mesothelial mass. Note the papillary arrangement of the neoplastic mesothelial cells supported by fibrous connective tissue. Mesothelial cells display a high degree of pleomorphism with nuclear atypia and few mitotic figures. Hematoxylin and eosin. Bar = 50 µm.

ABDOMINAL ULTRASONOGRAPHIC FINDINGS IN DOGS NATURALLY INFECTED WITH BABESIOSIS

EDUARDO FRAGA, JOSÉ DANIEL BARRERO, ANA GOICOA, LUCIANO ESPINO, GEMMA FRAGA, ANDRÉS BARRERO

Canine babesiosis is a tick-borne disease with a worldwide distribution that can involve multiple organs and result in a wide variety of clinical manifestations. Our goal was to describe the sonographic changes occurring in 72 dogs naturally infected with babesiosis. Seven healthy Beagle dogs were used as a control group. The most common finding in all dogs was splenomegaly with a diffuse heterogeneous parenchyma and generally reduced echogenicity. Diffuse hypoechoic hepatomegaly and bilaterally increased cortical echogenicity of the renal parenchyma were found more frequently in severe uncomplicated and complicated babesiosis groups. Mean renal resistive index (RI) values were 0.66/1.35, 0.73/1.91, and 0.71/1.73 for mild uncomplicated, severe uncomplicated, and complicated babesiosis groups, respectively. A markedly increased RI for complicated and severe uncomplicated groups correlated with anemia and severity of renal damage. Ultrasonography can be an adjunct for diagnosis and monitoring canine babesiosis and its systemic complication. The detection of diffuse heterogeneous splenomegaly can support the diagnosis of *Babesia* infection, because of the high prevalence of this lesion in these patients. © 2010 *Veterinary Radiology & Ultrasound*, Vol. 52, No. 3, 2011, pp 323-329.

Key words: abdominal ultrasonography, babesiosis, dog.

Vol. 52, No. 3

ULTRASONOGRAPHY IN CANINE BABESIOSIS

323

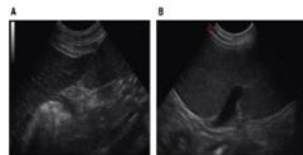


Fig. 2. Diffuse splenomegaly (arrows) is to the left of the image (A) Sagittal image in the mid abdomen. The spleen is enlarged and has rounded edges. (B) Image in the left negative abdomen. Note the marked convexity beneath the splenic venous insertion, indicating splenomegaly.

¿CUÁL ES TU DIAGNÓSTICO?

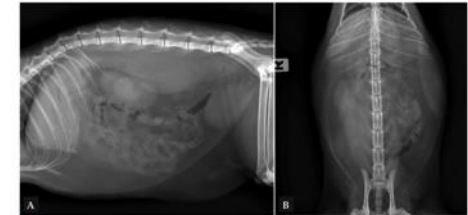


Figure 1. (A) Radiografía lateral y (B) ventrodorsal de abdomen de un gato que se presenta con dolor abdominal.

Historia clínica

Se presenta en consulta un gato macho, no castrado, de 1,5 años con historial de anorexia y apatía de aparición aguda (hace 2 días), sin vómitos ni diarrea, que tiene acceso al exterior. Las vacunaciones y las desparasitaciones están al día. En la exploración física el único hallazgo relevante es fiebre con dolor de origen indeterminado en la palpación abdominal. En la analítica sanguínea se observa leucocitosis marcada en el hemograma ($18.6 \times 10^9/l$), rango $0.8-7 \times 10^9/l$), con bioquímica normal.

Se realizan radiografías de abdomen lateral (L) y ventrodorsal (Fig. 1) para investigar posibles causas del dolor abdominal y la fiebre asociada.

Describe las anomalías radiográficas que se observan.

¿Cuáles son los posibles diagnósticos diferenciales que plantearías en este caso?

¿Qué otras técnicas realizarías para llegar a un diagnóstico definitivo?

J. D. Barreiro-Vázquez,¹ M. Vila-Pastor,² A. Seoane-Mojón,³ A. Barreiro-Lois,⁴
A. González-Cantalapiedra,⁵ J. L. González-Fraga⁶

¹Servicio de DPI- HVU Ref Codina, ²Servicio de Cirugía- HVU Ref Codina, Facultad de Veterinaria - USC, Avda. Carballo Calero s/n, 27002 Lugo, ³Clinica Veterinaria Laracha, Rúa Santa Lucía, 42, 15145 A Laracha, A Coruña,

⁴Clinica Veterinaria Laracha, Rúa Santa Lucía, 42, 15145 A Laracha, A Coruña,

Contacto: pedriand@barreirovazquez.es



Actividad clínica del servicio de DPI

- ✓ Fauna marina
 - ✓ Fondos marinos (geología sedimentaria)
- ## Acuicultura



SEDIMENTARY GEOLOGY, 50(2), 2011

El uso de la Tomografía Computarizada (TC) como técnica sedimentaria: aplicación en testigos oceánicos de la Cuenca Interior de Galicia (NW margen Ibérico)

The use of the Computerized Tomography (CT) as a sedimentary technique: application in oceanic cores from the Galicia Interior Basin (NW Iberian margin)

Asno Mesa^{1(*)}, Pablo Aguiar^{1(*)}, José Daniel Barreiro^{1,2,3}, Guillermo Francis^{1,4}, Marta Pérez-Arbores^{1,5}, Andrés Barreiro Lois^{1,6,7} y Alfredo Iglesias^{1,8}

ANATOMIA HISTOLOGIA EMBRYOLOGIA

Cross-Sectional Anatomy, Computed Tomography and Magnetic Resonance Imaging of the Thoracic Region of Common Dolphin (*Delphinus delphis*) and Striped Dolphin (*Stenella coeruleoalba*)

J. M. Alonso-Fariña¹, M. González-Ordén², J. D. Barreiro-Vázquez³, M. A. Aguiar⁴, A. Barreiro Lois⁵, J. M. Lorenzo-Fariña⁶ and E. Degollada⁷

*Correspondence:

Asno Mesa (E-mail: asno@ccma.es)

Asno Mesa (E-mail: asno@ccma.es)

Asno Mesa (E-mail: asno@ccma.es)

Asno Mesa (E-mail: asno@ccma.es)

Asno Mesa (E-mail: asno@ccma.es)

Asno Mesa (E-mail: asno@ccma.es)

Asno Mesa (E-mail: asno@ccma.es)

Asno Mesa (E-mail: asno@ccma.es)

Asno Mesa (E-mail: asno@ccma.es)

Asno Mesa (E-mail: asno@ccma.es)

Asno Mesa (E-mail: asno@ccma.es)

Asno Mesa (E-mail: asno@ccma.es)

Asno Mesa (E-mail: asno@ccma.es)

Asno Mesa (E-mail: asno@ccma.es)

Asno Mesa (E-mail: asno@ccma.es)

Asno Mesa (E-mail: asno@ccma.es)

Asno Mesa (E-mail: asno@ccma.es)

Asno Mesa (E-mail: asno@ccma.es)

Asno Mesa (E-mail: asno@ccma.es)

Asno Mesa (E-mail: asno@ccma.es)

Asno Mesa (E-mail: asno@ccma.es)

Asno Mesa (E-mail: asno@ccma.es)

Asno Mesa (E-mail: asno@ccma.es)

Asno Mesa (E-mail: asno@ccma.es)

Asno Mesa (E-mail: asno@ccma.es)

Asno Mesa (E-mail: asno@ccma.es)

Asno Mesa (E-mail: asno@ccma.es)

Asno Mesa (E-mail: asno@ccma.es)

Asno Mesa (E-mail: asno@ccma.es)

Asno Mesa (E-mail: asno@ccma.es)

Asno Mesa (E-mail: asno@ccma.es)

Asno Mesa (E-mail: asno@ccma.es)

Asno Mesa (E-mail: asno@ccma.es)

ANATOMIA HISTOLOGIA EMBRYOLOGIA

Cross-sectional Anatomy, Computed Tomography and Magnetic Resonance Imaging of the Head of Common Dolphin (*Delphinus delphis*) and Striped Dolphin (*Stenella coeruleoalba*)

J. M. Alonso-Fariña¹, M. González-Ordén², J. D. Barreiro-Vázquez³, A. Barreiro Lois⁴, M. Andre⁵, M. Morell⁶, M. Llaneza-Rodrigo⁷, T. Mironov-Petrovsky⁸ and E. Degollada⁹

*Correspondence:

Asno Mesa (E-mail: asno@ccma.es)

Asno Mesa (E-mail: asno@ccma.es)

Asno Mesa (E-mail: asno@ccma.es)

Asno Mesa (E-mail: asno@ccma.es)

Asno Mesa (E-mail: asno@ccma.es)

Asno Mesa (E-mail: asno@ccma.es)

Asno Mesa (E-mail: asno@ccma.es)

Asno Mesa (E-mail: asno@ccma.es)

Asno Mesa (E-mail: asno@ccma.es)

Asno Mesa (E-mail: asno@ccma.es)

Asno Mesa (E-mail: asno@ccma.es)

Asno Mesa (E-mail: asno@ccma.es)

Asno Mesa (E-mail: asno@ccma.es)

Asno Mesa (E-mail: asno@ccma.es)

Asno Mesa (E-mail: asno@ccma.es)

Asno Mesa (E-mail: asno@ccma.es)

Asno Mesa (E-mail: asno@ccma.es)

Asno Mesa (E-mail: asno@ccma.es)

Asno Mesa (E-mail: asno@ccma.es)

Asno Mesa (E-mail: asno@ccma.es)

Asno Mesa (E-mail: asno@ccma.es)

Asno Mesa (E-mail: asno@ccma.es)

Asno Mesa (E-mail: asno@ccma.es)

Asno Mesa (E-mail: asno@ccma.es)

Asno Mesa (E-mail: asno@ccma.es)

Asno Mesa (E-mail: asno@ccma.es)

Asno Mesa (E-mail: asno@ccma.es)

Asno Mesa (E-mail: asno@ccma.es)

Asno Mesa (E-mail: asno@ccma.es)

Asno Mesa (E-mail: asno@ccma.es)

Asno Mesa (E-mail: asno@ccma.es)

Asno Mesa (E-mail: asno@ccma.es)

Asno Mesa (E-mail: asno@ccma.es)

Technical Anatomy and Imaging of Dolphin Tissues

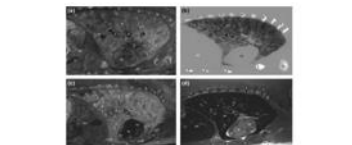


Fig. 1. High-resolution CT and MRI images of dolphin tissues, showing detailed anatomical structures of the thoracic region.

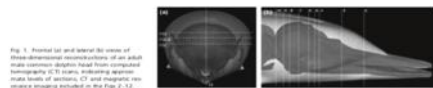


Fig. 2. Coronal CT and MRI scans of a common dolphin head, showing the internal anatomy of the skull and facial region.

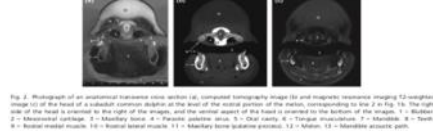


Fig. 3. Axial CT and MRI scans of a common dolphin head, showing cross-sectional views of the skull and facial region.

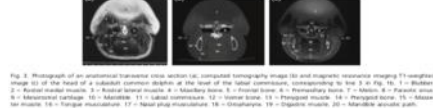


Fig. 4. Axial CT and MRI scans of a striped dolphin head, showing cross-sectional views of the skull and facial region.

Sedimentary Geology

A novel sedimentological method based on CT-scanning: Use for tomographic characterization of the Galicia Interior Basin

Asno Mesa¹, Guillermo Francis¹, Marta Pérez-Arbores¹, Pablo Aguiar¹, José Daniel Barreiro-Vázquez¹, Alfredo Iglesias¹, Andrés Barreiro Lois¹

ARTICLE INFO

Received 15 March 2011

Accepted 15 March 2011

Article published online 15 March 2011

Issue 2, July 2011

Pages 151-161

DOI: 10.1016/j.sedgeo.2011.03.001

Keywords: CT-scanning, sedimentology, Galicia Interior Basin

Abstract: A novel sedimentological method based on CT-scanning is presented. The method consists in the use of CT-scanning to obtain high-resolution images of sedimentary cores. The images are then processed to obtain tomographic slices, which are used to characterize the sedimentary facies and to identify the sedimentary structures. The method is applied to the Galicia Interior Basin, NW Iberian margin, and the results are compared with those obtained by conventional sedimentological methods.

ABSTRACT

A novel sedimentological method based on CT-scanning is presented. The method consists in the use of CT-scanning to obtain high-resolution images of sedimentary cores. The images are then processed to obtain tomographic slices, which are used to characterize the sedimentary facies and to identify the sedimentary structures. The method is applied to the Galicia Interior Basin, NW Iberian margin, and the results are compared with those obtained by conventional sedimentological methods.

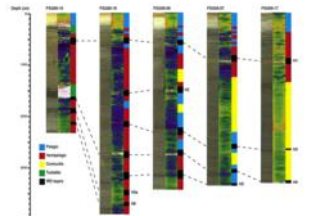


Fig. 5. A series of vertical tomographic slices showing sedimentary facies and structures, with a color-coded legend indicating different sediment types.

Actividad clínica del servicio de DPI

Fauna marina

Fondos marinos (geología sedimentaria)

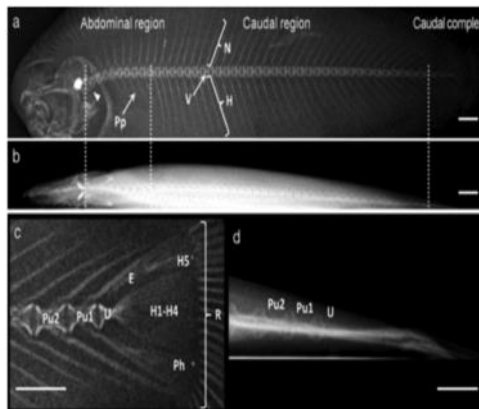
✓ Acuicultura

Vol. 124, 117–126, 2017 https://doi.org/10.3354/dm043110	DISEASES OF AQUATIC ORGANISMS Dis Aquat Org	Published April 20
---	--	--------------------

Skeletal anomalies in reared Senegalese sole *Solea senegalensis* juveniles: a radiographic approach

A. M. de Azevedo¹*, A. P. Losada¹, A. Barreiro^{1,2}, J. D. Barreiro^{1,2}, I. Ferreiro¹,
A. Ríaza³, S. Vázquez¹, M. I. Quiroga¹

¹Departamento de Anatomía, Producción Animal y Ciencias Clínicas Veterinarias, Facultad de Veterinaria, Universidad de Santiago de Compostela, Lugo 27002, Spain
²Hospital Veterinario Universitario Ref Codina, Lugo 27002, Spain
³Stoll Sea Farm, A Cerua 15292, Spain

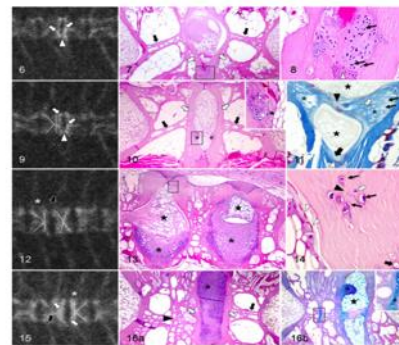


Original Article
Skeletal Anomalies in Senegalese Sole (*Solea senegalensis*), an Anosteocytic Boned Flatfish Species

Ana Manuela de Azevedo¹, Ana Paula Losada¹, Andrés Barreiro^{1,2}, Sonia Vázquez¹, and María Isabel Quiroga¹

Abstract
Skeletal anomalies affect animal welfare and cause important economic problems in aquaculture. Despite the high frequency of skeletal problems in reared *Solea senegalensis*, there is lack of information regarding the histological features of normal and deformed vertebrae in this flatfish. The aim of this study was to describe the histopathological and radiographic appearance of vertebral body anomalies. Sixty-seven juvenile fish were radiographically assessed 104 to 109 days after hatching. Through radiographic images, vertebral segments were selected and processed for histopathological examination from 7 normal and 2 affected fish. Alterations in bone shape and mineralization were the most significant anomalies in the vertebral bodies. These alterations occurred most frequently between the last 3 abdominal vertebrae and the first 10 caudal spines. Radiographically, deformed vertebrae showed flattening of the endplates and narrowing of the intervertebral spaces. The radiographic findings concurred with the histological lesions where affected vertebrae exhibited irregular endplates and changes in trabecular bone. Radiolucid cartilaginous tissue was evident in the endplates of the deformed vertebrae and, in some cases, the cartilaginous material extended from the growth zone into the intervertebral space. These changes were likely the primary alterations that led to vertebral fusion. Fused vertebrae were often radiolucid and showed a morphogenesis of the vertebrae. The formation of metaplastic cartilage is frequent in a variety of anomalies affecting teleost species.

Keywords
osteocytic bone, fish, histopathology, Senegalese sole (*Solea senegalensis*), skeletal anomalies, vertebrae



Figures 2–14. Deformed vertebrae, *Solea senegalensis*. **Figure 2.** Lateral radiographic projection (L) of deformed centra displaying flattened and radiolucid endplates (white arrows) that were fused (white outline) to each other. The intervertebral space (IVS) is narrowed and radiolucid (Fig. 2). **Figure 3.** Histological section of the same segment as in Fig. 2. Abnormal and radiolucid endplates (white arrows) in a ventral view, forming a lamina rotatoria. The endplates (white arrows) are anastomosed both in the cranial–caudal axis and in the dorsoventral axis. Note the presence of radiolucid tissue in the proximity of the growth zone (metaplastic, metaplastic and non-IVS). **Figure 4.** Radiolucid tissue in the area of the vertebrae (Fig. 4). **Figure 5.** Cartilage near the growth zone (white arrowheads) and the vertebrae. Chondrocytes (black arrows) are evident in lacunae, surrounded by abundant cartilaginous extracellular matrix (ECM). **Figure 6.** L1 showing alterations of the vertebral intervertebral structures as “C”-like vertebrae (black lines) and opposing flattened and radiolucid endplates (white arrows). The IVS is radiolucid and, in 2 points, the endplates fused with each other (white arrowheads). **Figure 7.** Section from the same segment as in Fig. 9. Oblique longitudinal trabeculae (black arrows) and flattened endplates (white arrows) in being vertebrae, showing protrusion of these trabeculae (white dots) towards the centrum (V). **Figure 8.** Transverse radiographic projection of the same segment showing protrusion of these trabeculae (white dots) towards the centrum (V). **Figure 9.** Right side of the same segment as in Fig. 10. A blue line marks indication of fused (white arrow) towards chondrocytes (black arrows) in the

November 1986–001 (2017), 969–972
Contents lists available at ScienceDirect
Aquaculture
Journal homepage: www.elsevier.com/locate/aqua-online

Short communication
Induction of triploidy in turbot (*Scophthalmus maximus*) does not affect gross body morphology and skeleton characteristics
Jorge Hernández-Urcera^a, Eva Torres^a, Daniel Barreiro^a, Andrés Barreiro-Luis^a, Josep Alsius^b, Rita Gal^c, Josep Ballarín^{b,*}

^a Instituto Español de Acuicultura (IEA), Centro Investigador de Fijado, 46100 Sagunto, Spain
^b Departament d'Enginyeria i Ciències de l'Alimentació i Nutrició (ENAN), Universitat de València, 46100 Sagunto, Spain
^c IRTA, 08209 Sabadell, Spain

ARTICLE INFO
Article history:
Received 26 July 2016
Received in revised form 17 January 2017
Accepted 22 January 2017
Available online 13 February 2017

ABSTRACT
Digital images (Scophthalmus maximus) produced by cold shock showed no differences in their gross body morphology and skeleton characteristics compared with their diploid fish.
© 2017 Elsevier B.V. All rights reserved.

312 J. Hernández-Urcera et al. / Aquaculture

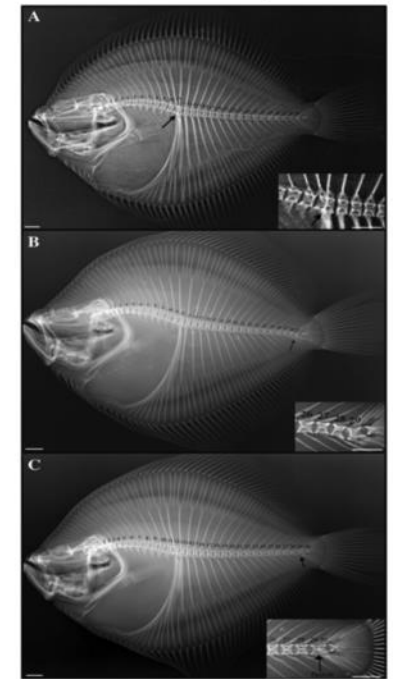
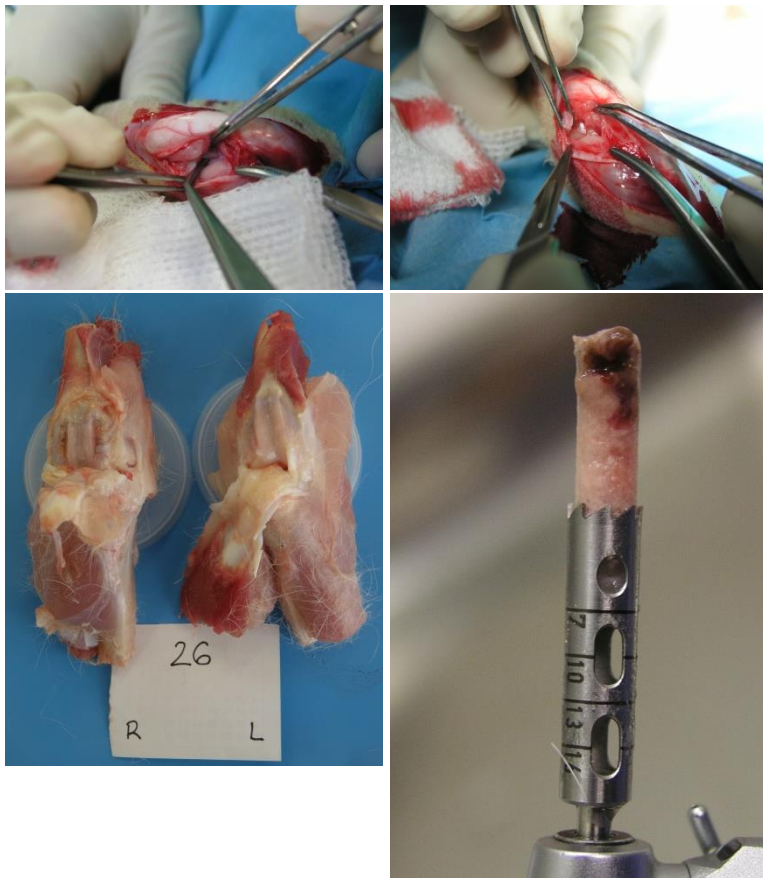


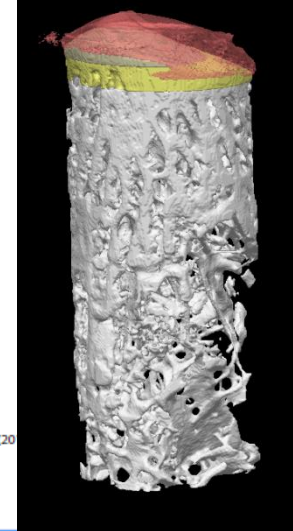
Fig. 4. Radiographic images of turbot at 12 months from the triploid group. Enlarged picture (bottom to the right) corresponds to the most common malformed areas. Scale bar, 1 cm.




Realización de pruebas in vivo:

Osteoartrosis



Permuy et al. BMC Veterinary Research (2018) 12:1186
DOI 10.1186/s12917-018-0458-x



-  Subchondral bone
-  Trabecular bone
-  Articular cartilage



RESEARCH ARTICLE

Open Access



Effects of diacerein on cartilage and subchondral bone in early stages of osteoarthritis in a rabbit model

María Permuy^{1*}, David Guede², Mónica López-Peña¹, Fernando Muñoz¹, Jose-Ramón Caero³

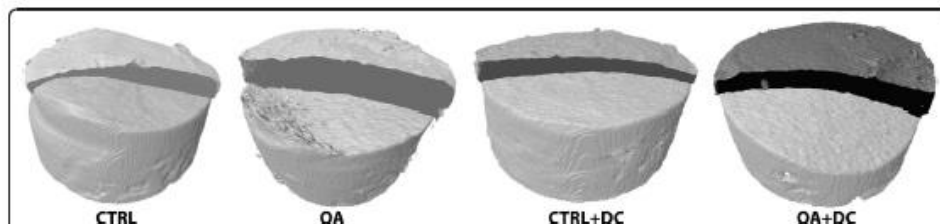
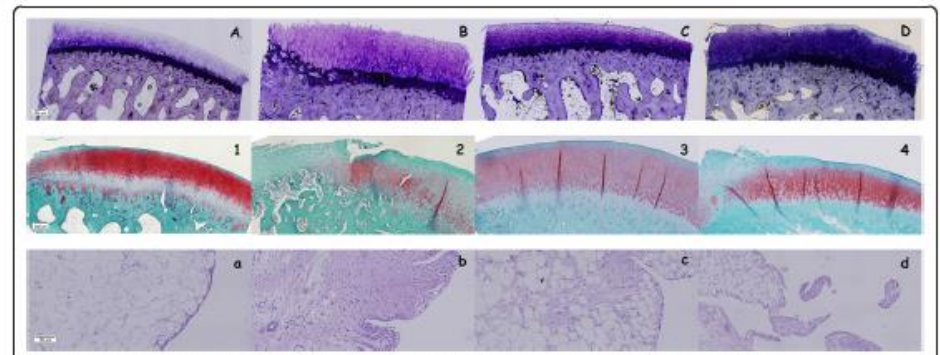


Figure 5 Micro-CT 3D models of a representative sample of each experimental group. Cartilage swelling characteristic of the first stages of OA can be clearly appreciated in OA samples, whereas diacerein-treated samples recover normal cartilage morphology like CTRL.

Realización de pruebas in vivo:

Cardiotoxicidad



Subacute Cardiotoxicity of Yessotoxin: *In Vitro* and *In Vivo* Studies

Sara F. Ferreiro,[†] Natalia Vilarinho,^{*†} Cristina Carrera,^{†,§} M. Carmen Louzao,[†] Antonio G. Cantalapiedra,^{‡,§} Germán Santamarina,^{‡,§} J. Manuel Cifuentes,^{||} Andrés C. Vieira,[†] and Luis M. Botana^{*†}

[†]Departamento de Farmacología, [‡]Departamento de Ciencias Clínicas Veterinarias, [§]Hospital Veterinario Universitario Rof Codina and ^{||}Departamento de Anatomía y Producción Animal, Facultad de Veterinaria, Universidade de Santiago de Compostela, 27002 Lugo, Spain

Author's Personal Copy

Toxicol 129 (2017) 74–80



Contents lists available at ScienceDirect

Toxicol

journal homepage: www.elsevier.com/locate/toxicol



Subacute immunotoxicity of the marine phycotoxin yessotoxin in rats



Sara F. Ferreiro^a, Natalia Vilarinho^{a,**}, Cristina Carrera^{a,c}, M. Carmen Louzao^a, Germán Santamarina^{b,c}, Antonio G. Cantalapiedra^{b,c}, J. Manuel Cifuentes^d, Andrés C. Vieira^a, Luis M. Botana^{a,*}

^a Departamento de Farmacología, Facultad de Veterinaria, Universidad de Santiago de Compostela, 27002 Lugo, Spain

^b Departamento de Ciencias Clínicas Veterinarias, Facultad de Veterinaria, Universidad de Santiago de Compostela, 27002 Lugo, Spain

^c Hospital Veterinario Universitario Rof Codina, Facultad de Veterinaria, Universidad de Santiago de Compostela, 27002 Lugo, Spain

^d Departamento de Anatomía y Producción Animal, Facultad de Veterinaria, Universidad de Santiago de Compostela, 27002 Lugo, Spain

Author's personal copy

Arch Toxicol (2014) 88:425–434
DOI 10.1007/s00204-013-1115-4

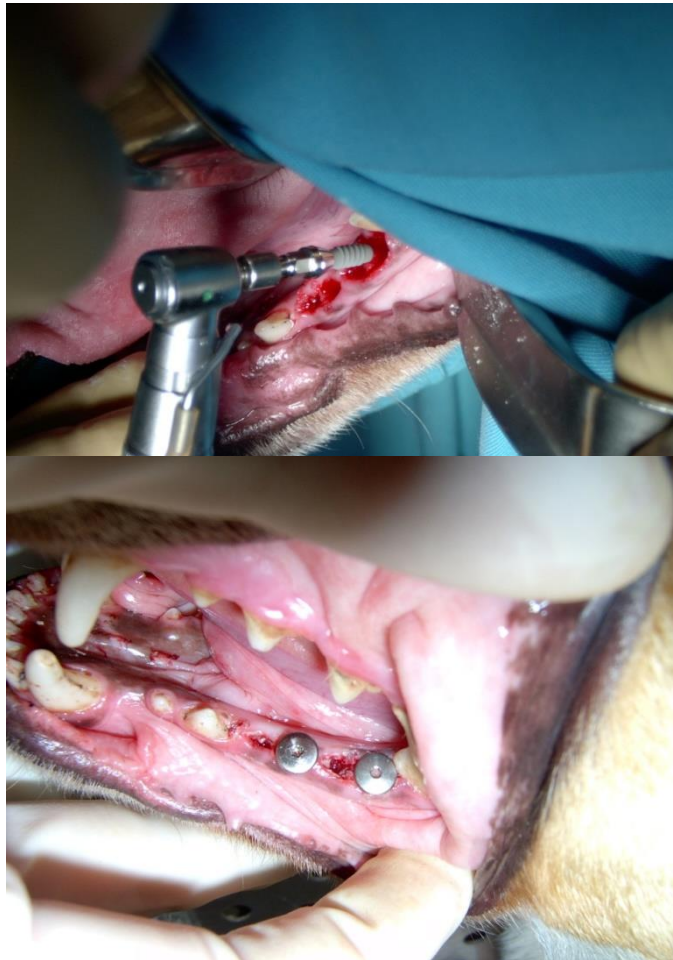
ORGAN TOXICITY AND MECHANISMS

In vivo arrhythmogenicity of the marine biotoxin azaspiracid-2 in rats

Sara F. Ferreiro · Natalia Vilarinho · Cristina Carrera · M. Carmen Louzao · Germán Santamarina · Antonio G. Cantalapiedra · Laura P. Rodríguez · J. Manuel Cifuentes · Andrés C. Vieira · K. C. Nicolaou · Michael O. Frederick · Luis M. Botana

Realización de pruebas in vivo:

Osteointegración implantes dentales



Goran I. Benic
Daniel S. Thoma
Ronald E. Jung
Ignacio Sanz-Martin
Silvan Unger
Antonio Cantalapiedra
Christoph H.F. Hämmerle

Author affiliations:

Goran I. Benic, Daniel S. Thoma, Ronald E. Jung, Silvan Unger, Christoph H.F. Hämmerle, Clinic of Fixed and Removable Prosthodontics and Dental Material Science, Center of Dental Medicine, University of Zurich, Zurich, Switzerland
Antonio Cantalapiedra, Faculty of Veterinary, University of Santiago de Compostela, Santiago, Spain
Ignacio Sanz-Martin, Faculty of Odontology, Universidad Complutense de Madrid, Madrid, Spain

Corresponding author:

Dr. Goran I. Benic
Clinic of Fixed and Removable Prosthodontics and Dental Material Science
Center of Dental Medicine
University of Zurich
Plattenstrasse 11, 8033 Zurich, Switzerland
Tel.: +41 44 634 23 60
Fax: +41 44 634 48 00
e-mail: goran.benic@zsm.unizh.ch

Date:

Accepted 11 February 2017

To cite this article:

Benic GI, Thoma DS, Jung RE, Sanz-Martin I, Unger S, Cantalapiedra A, Hämmerle CHF. Guided bone regeneration with particulate bovine bone substitute: a pilot canine beam computed tomographic investigation. *Clin Oral Implants Res*. 2017; doi:10.1111/clir.12911

©

Daniel S. Thoma
Goran I. Benic
Fernando Muñoz
Ralf Kobal
Ignacio Sanz-Martin
Antonio G. Cantalapiedra
Christoph H. F. Hämmerle
Ronald E. Jung

Author affiliations:

Daniel S. Thoma, Goran I. Benic, Christoph H.F. Hämmerle, Ronald E. Jung, Clinic for Fixed and Removable Prosthodontics and Dental Material Science, University of Zurich, Zurich, Switzerland
Fernando Muñoz, Antonio G. Cantalapiedra, Department of Veterinary Clinical Science, University of Santiago de Compostela, Lugo, Spain
Ralf Kobal, Department of Prosthodontics, Allertalstraße University, Heching, Germany
Ignacio Sanz-Martin, Universidad Complutense, Madrid, Spain

Corresponding author:

Dr. Daniel S. Thoma
Clinic of Fixed and Removable Prosthodontics and Dental Material Science
Center of Dental Medicine
University of Zurich, Mattenstrasse 11,
CH-8033 Zurich, Switzerland
Tel.: +41 44 634 33 60
Fax: +41 44 634 48 00
e-mail: daniel.thoma@zsm.unizh.ch

Date:

Accepted 4 March 2017

To cite this article:

Thoma DS, Benic GI, Muñoz F, Jung RE, Sanz-Martin I, Cantalapiedra AG, Hämmerle CHF. Guided bone regeneration with particulate bovine bone substitute: a pilot canine beam computed tomographic investigation. *Clin Oral Implants Res*. 2017; doi:10.1111/clir.12911

Guided bone regeneration with particulate vs. block xenogenic bone substitutes: a pilot cone beam computed tomographic investigation

Key words: alveolar ridge augmentation, alveolar ridge defect, animal study, block, bone, bone graft, bone substitute, cone beam computed tomography, dental implants, guided bone regeneration, membrane

Abstract

Aims: To test whether an equine bone substitute block used for guided bone regeneration (GBR) of peri-implant defects differs from bovine block or particulate bone substitutes regarding the hard and soft tissue contours of the augmented ridge.
Material & Methods: Two semi-saddle bone defects were prepared in each side of the mandible of eight dogs, and one titanium implant was inserted into every defect. The defects were randomly allocated to receive one of the following treatments: bone augmentation by GBR using (1) particulate deproteinized bovine bone mineral (DBBM) + a collagen membrane (CM), (2) block DBBM + CM, (3) equine bone substitute block + CM, and (4) empty control. After 4 months, the jaws were scanned by means of cone beam computed tomography (CBCT). CBCT analysis was performed in one central and two lateral (anterior and distal) regions of interest (ROI) of each site evaluating the horizontal thickness of the augmented hard tissue (HT_{aug}) and the total thickness of hard and soft tissue (HT_{total}). The Wilcoxon-Mann signed rank test was used for statistical analysis.

Results: In the majority of ROI, equine and bovine blocks rendered significantly higher values in HT_{aug} and HT_{total} than controls ($P < 0.05$). Generally, equine blocks reached the highest values in HT_{aug} and HT_{total} followed by DBBM blocks and particulate DBBM. The differences in HT_{aug} and HT_{total} between GBR groups were not statistically significant ($P > 0.05$). In the central ROI, HT_{aug} at the level of the implant shoulder measured 1.7 ± 1.8 mm for equine blocks, 1.7 ± 1.0 mm for DBBM blocks, 0.9 ± 1.2 mm for particulate DBBM, and 0 ± 0 mm for control. The corresponding values in the lateral ROI reached 1.9 ± 1.1 mm for equine blocks, 1.2 ± 0.8 mm for DBBM blocks, 1.0 ± 0.9 mm for particulate DBBM, and 0 ± 0 mm for control. **Conclusions:** GBR with bone substitute blocks lead to higher ridge dimensions than empty control. The equine block with CM rendered the most favorable outcomes in hard and soft tissue contours followed by DBBM block and DBBM granulate with CM.

Guided bone regeneration (GBR) is the best method to augment bone in localized alveolar defects (Benic & Hämmerle 2014). There is a large body of clinical evidence documenting the long-term success of dental implants placed in combination with GBR (Hämmerle et al. 2002; Driess et al. 2009; Jensen & Terheyden 2009). In contrast, there is insufficient amount of information on the hard and soft tissue contour changes of the augmented ridge.

With regard to the choice of the biomaterial for GBR, currently, the use of particulate xenogenic bone substitutes in combination with collagen membranes (CM) is the most common and documented method for the augmentation of peri-implant defects (Chiapasco & Zanussi 2009; Jensen & Terheyden 2009). Recent cone beam computed tomographic investigations of peri-implant defects treated with particulate xenogenic bone substitute with or without collagen membranes showed no combination with CM found

CLINICAL ORAL IMPLANTS RESEARCH

Marginal bone-level alterations of loaded zirconia and titanium dental implants: an experimental study in the dog mandible

Key words: bone, crown, dental implants, titanium, X-rays, zirconium oxide

Abstract

Objectives: The aim was to test whether or not the marginal bone-level alterations of loaded zirconia implants are similar to the bone-level alterations of a grade 4 titanium oxypitane dental implant.

Materials and methods: In six dogs, all premolars and the first molars were extracted in the mandible. Four months later, two zirconia implants (BP, VC, 20) and a control titanium oxypitane (STM) implant were randomly placed in each hemimandible and left for transmaxillary healing (baseline). Six months later, CAD/CAM crowns were cemented. Sacrifice was scheduled at 6-month postloading. Digital X-rays were taken at implant placement, crown insertion, and sacrifice. Marginal bone level alterations were calculated, and intra- and intergroup comparisons performed adjusted by confounding factors.

Results: Implants were successfully placed. Until crown insertion, two implants were fractured (one VC, one 20). At sacrifice, 5 more implants were (partly) fractured (one BP, four 20), and one lost osteointegration (VC). No decementation of crowns occurred. All implant systems demonstrated a statistically significant (except VC) loss of marginal bone between baseline and crown insertion ranging from 0.29 mm (VC; $P = 0.110$) to 1.80 mm (20; $P = 0.018$). The estimated marginal bone loss between baseline and 6 months of loading ranged between 0.80 mm (BP) and 1.11 mm (VC), being statistically significant for STM and VC only ($P < 0.05$). The changes in marginal bone levels were statistically significantly different between zirconia implants and control implants (STM vs. BP; $P = 0.007$; vs. VC; $P = 0.001$; vs. 20; $P = 0.011$).

Conclusions: Zirconia implants were more prone to fracture prior to and after loading with implant supported dentures compared to titanium implants. Individual differences and variability in the extent of the bone-level change during the 12-month study period were found between the different implant types and materials.

Dental implants have become a predictable treatment modality for the replacement of single or multiple missing teeth (Patterson et al. 2012). Titanium and titanium alloys are considered a gold standard and the material of choice due to favorable physico-chemical properties and their biologic attributes (osteointegration) (Schroeder et al. 1976; Birkmeyer et al. 1977). Numerous preclinical and clinical studies have documented successful hard and soft tissue integration of titanium and titanium alloy implants with predictably high survival rates over 10 years (Buser et al. 1997, 2003; Abrahamson & Wen-

nerberg 2004; Attar & Zarb 2004; Ramonsson et al. 2005; Abrahamson & Carlsson 2007).

Some limitations apply, as it has been shown that during clinical function, soft tissue shrinkage, recession, and post-implant lesions can leave the implant head visible (Cisarow 2000; Cantalapiedra et al. 2006). In Birkmeyer et al. (1977), numerous preclinical and clinical studies have documented successful hard and soft tissue integration of titanium and titanium alloy implants with predictably high survival rates over 10 years (Buser et al. 1997, 2003; Abrahamson & Wen-

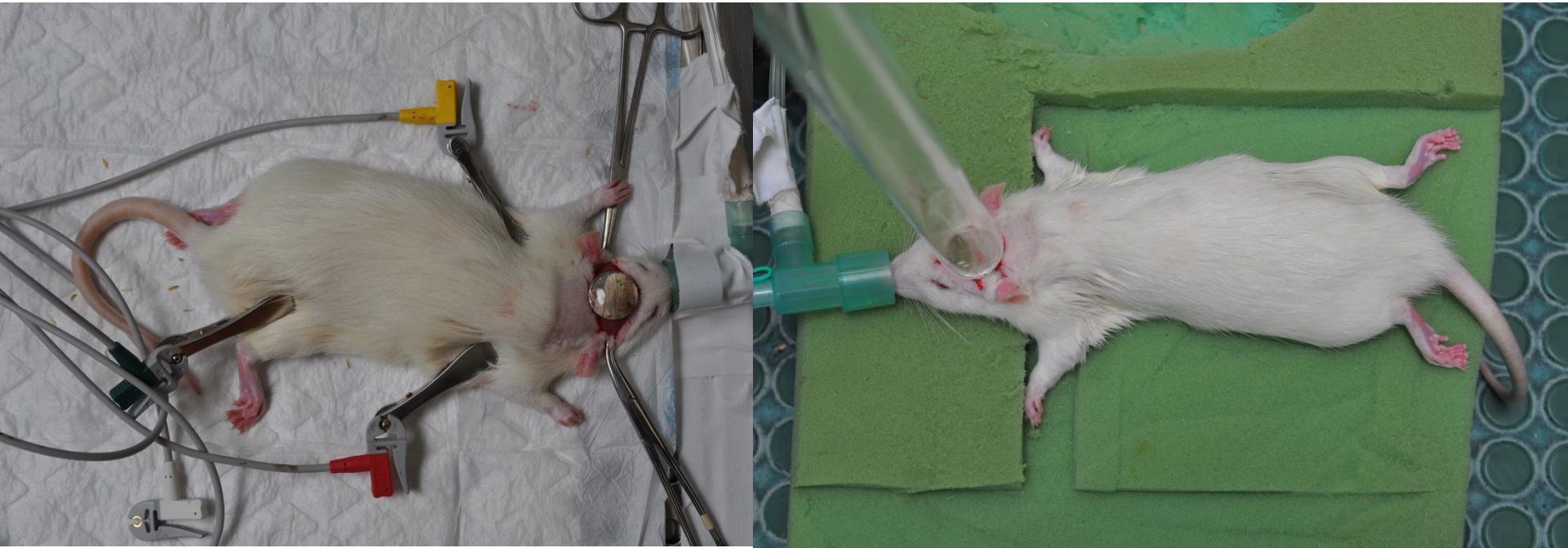
Realización de pruebas in vivo:

Osteointegración biomateriales en calota



Realización de pruebas in vivo:

Daño axonal difuso traumático/isquémico



Realización de pruebas in vivo:

Tejido adiposo blanco/marrón



Research

Z LÓPEZ-IBARRA and others

Adipose tissue energetic metabolism

54:2

105–113

Metabolic differences between white and brown fat from fasting rabbits at physiological temperature

Z López-Ibarra¹, J Modrego², M Valero-Muñoz³, P Rodríguez-Sierra², J J Zamorano-León², A González-Cantalapiedra¹, N de las Heras^{2,3}, S Ballesteros^{2,3}, V Lahera^{2,3} and A J López-Farré^{2,4}

¹Surgery Department, Hospital Universitario ROF-Codina, Lugo, Spain

²Instituto de Investigación Sanitaria del Hospital Clínico San Carlos (IIBS), Madrid, Spain

³Department of ³Rheumatology and ⁴Medicine, School of Medicine, Universidad Complutense de Madrid

Correspondence should be addressed to A J López-Farré or V Lahera
Emails: sif@telefonos.net or

ARCHIVES OF PHYSIOLOGY AND BIOCHEMISTRY, 2017
<https://doi.org/10.1080/13813455.2017.1360913>

Taylor & Francis
Taylor & Francis Group

ORIGINAL ARTICLE

Check for updates

Really does temperature reduction and norepinephrine have similar effects on the energy metabolism in rat brown adipose tissue?

B. Sopena^{a,*}, Z. López-Ibarra^{a,b,*}, A. J. López-Farré^a, N. de las Heras^c, S. Ballesteros^c, A. González-Cantalapiedra^b, V. Lahera^c and J. J. Zamorano-León^a

^aDepartment of Medicine, School of Medicine, Universidad Complutense de Madrid, Madrid, Spain; ^bSurgery Department, Hospital Universitario ROF-Codina, Lugo, Spain; ^cDepartment of Physiology, School of Medicine, Universidad Complutense de Madrid, Madrid, Spain

ABSTRACT

Context: Heat generation by brown adipose tissue (BAT) in response to temperature reduction seems to be entirely related to sympathetic nervous stimulation.

Objective: To analyse if temperature reduction and norepinephrine may differently affect the expression of proteins related to energy metabolism in BAT.

Materials and methods: Isolated rats BAT was incubated with/without norepinephrine (10⁻⁶ mol/L, 24 h at 32 °C and 37 °C).

Results: In BAT, 32 °C increased the protein expression levels of carnitine palmitoyltransferase-I and -II, mitochondrial uncoupling protein-1 (UCP-1) and the expression and activity of lactate dehydrogenase. Mitochondrial F₁-ATP synthase α -chain expression was decreased at 32 °C compared to 37 °C. Norepinephrine and at 32 °C exposure, UCP-1 expression was increased but cytochrome-c oxidase and F₁-ATP synthase α -chain expression was reduced with respect to 37 °C.

Discussion: Sympathetic stimulation seems not to be the only factor associated with heat generation.

Conclusions: Temperature reduction by itself exerts some different effects on the expression of proteins related to the energy metabolism than norepinephrine.

ARTICLE HISTORY

Received 5 June 2017
Revised 19 July 2017
Accepted 24 July 2017
Published online 25 August 2017

KEYWORDS

Brown adipose tissue; β -oxidation; mitochondrial oxidative phosphorylation; norepinephrine; temperature reduction

Osteointegración

J Clin Periodontol 2015; 42: 967–975 doi: 10.1111/jcpe.12453

Journal of
Clinical
Periodontology

Odontology
<https://doi.org/10.1007/s10266-018-0384-z>

ORIGINAL ARTICLE



Evaluation of a new tricalcium phosphate for guided bone regeneration: an experimental study in the beagle dog

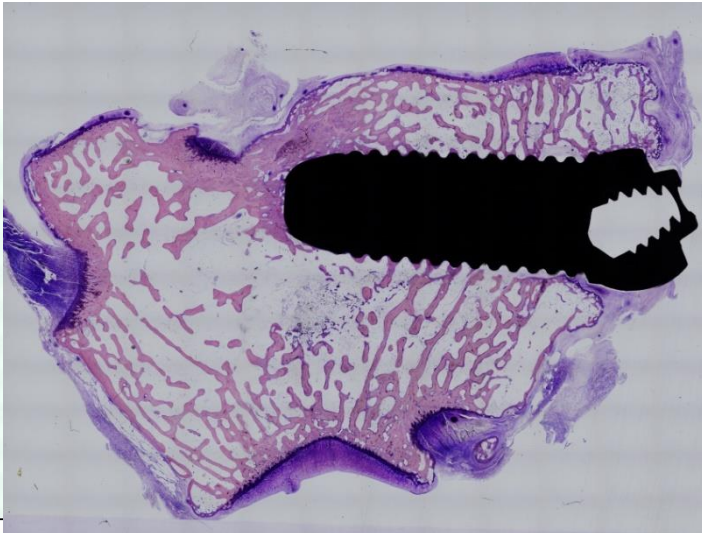
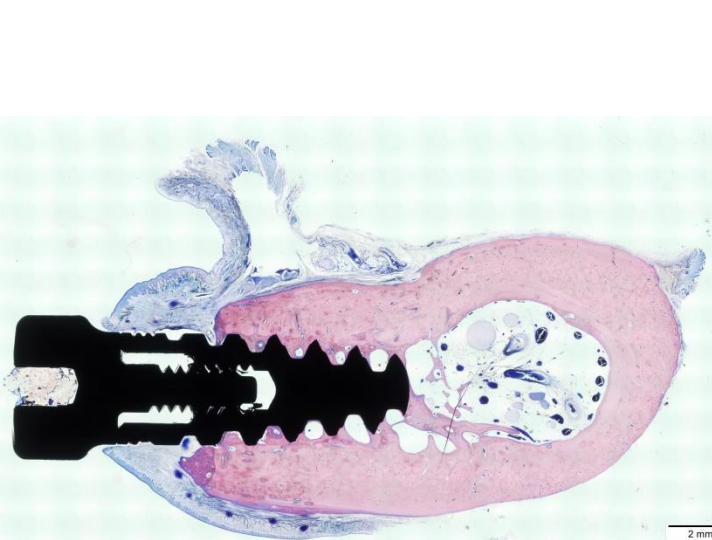
Mario Pérez-Sayáns^{1,2} · Alejandro I. Lorenzo-Pouso^{1,2} · Pablo Galindo-Moreno³ · Fernando Muñoz-Guzón⁴ · Antonio González-Cantalapiedra⁴ · Mónica López-Peña⁴ · Manuel Somoza-Martín¹ · Mercedes Gallas-Torreira¹ · Abel García-García^{1,2}

Received: 25 June 2018 / Accepted: 1 August 2018
© The Society of The Nippon Dental University 2018

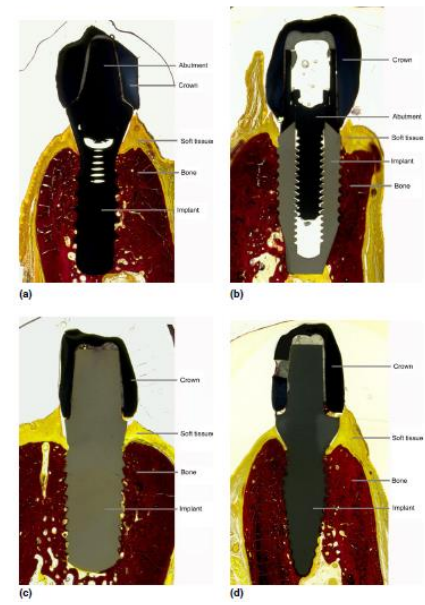
Histological analysis of loaded zirconia and titanium dental implants: an experimental study in the dog mandible

Daniel S. Thoma¹, Goran I. Benic¹, Fernando Muñoz², Ralf Kohal³, Ignacio Sanz Martín⁴, Antonio González Cantalapiedra², Christoph H. F. Hammerle¹ and Ronald E. Jung¹
¹Clinic of Fixed and Removable Prosthodontics and Dental Material Science, University of Zurich, Zurich, Switzerland; ²Department of Velefary Clinical Sciences, University of Santiago de Compostela, Lugo, Spain; ³Department of Prosthodontics, Albert-Ludwigs-University, Freiburg, Germany; ⁴Universidad Complutense, Madrid, Spain

Thoma DS, Benic GI, Muñoz F, Kohal R, Sanz Martín I, Cantalapiedra AG, Hammerle CHF, Jung RE. Histological analysis of loaded zirconia and titanium dental implants: an experimental study in the dog mandible. *J Clin Periodontol* 2015; 42: 967–975. doi: 10.1111/jcpe.12453

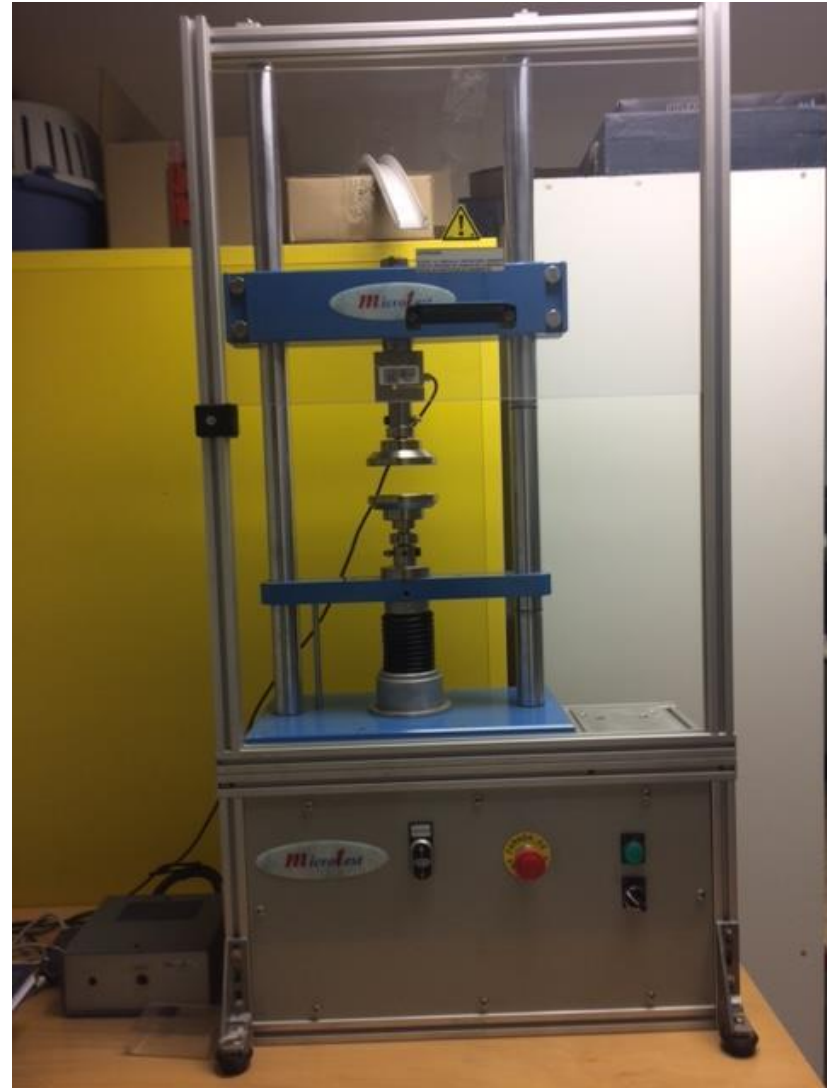
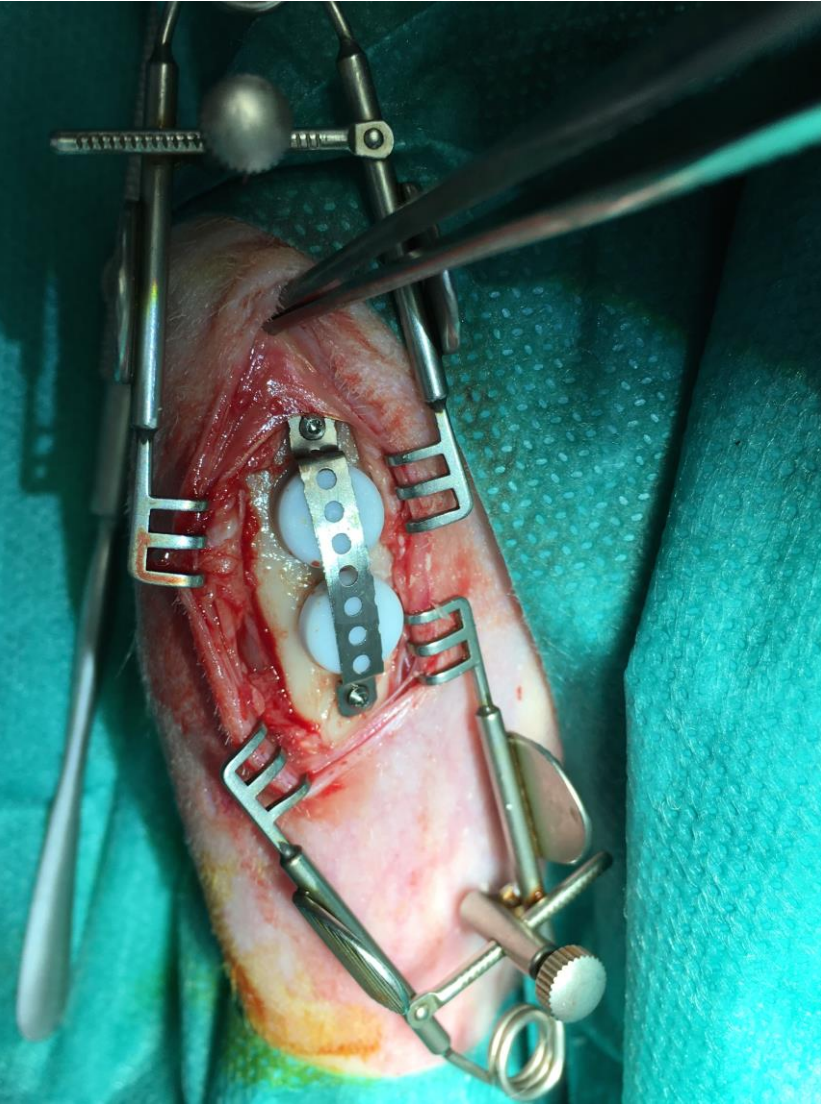


972 Thoma et al.



Laboratorio investigación:

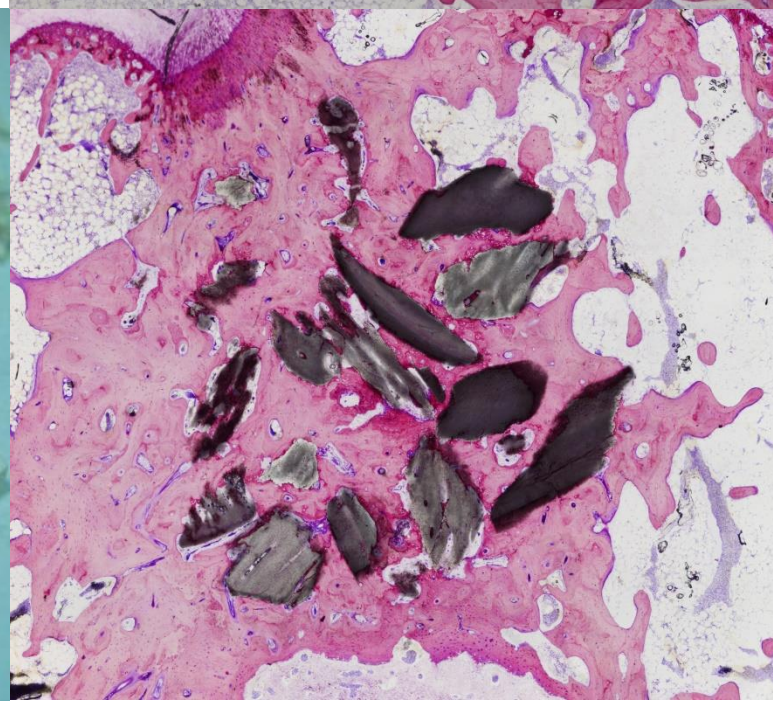
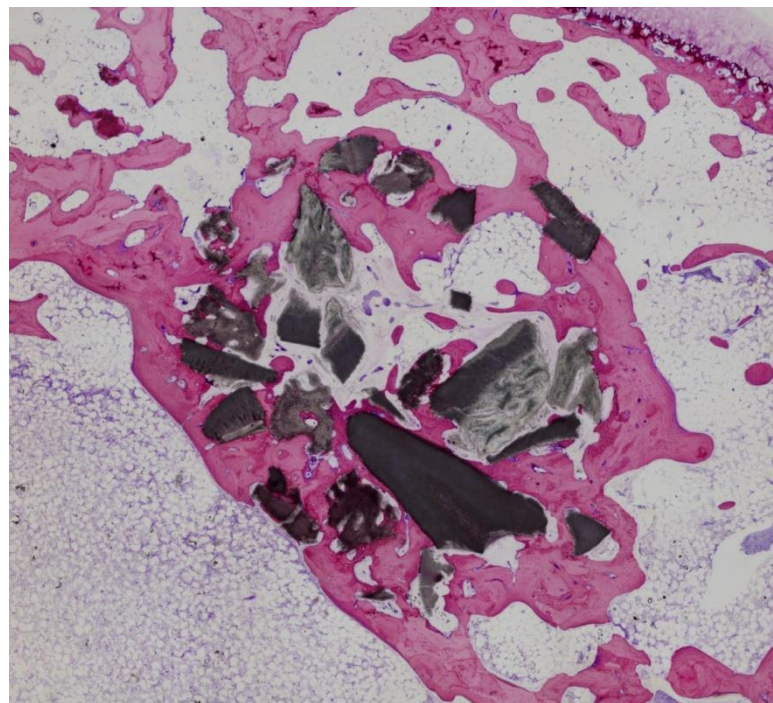
Osteointegración: test de tracción



Laboratorio investigación:

BIOMATERIALES

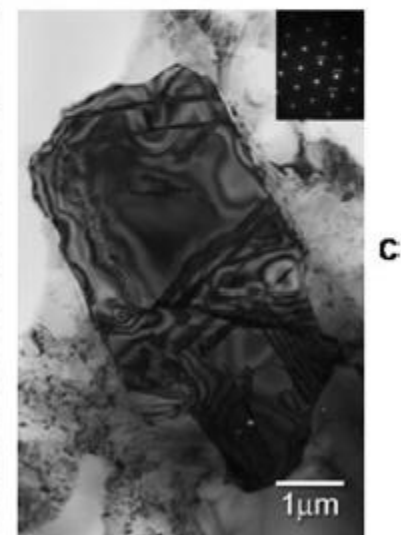
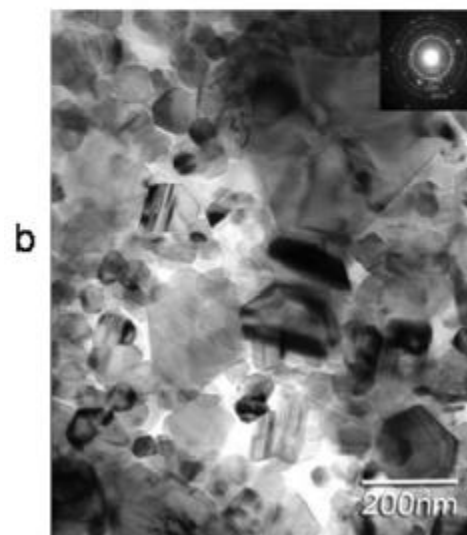
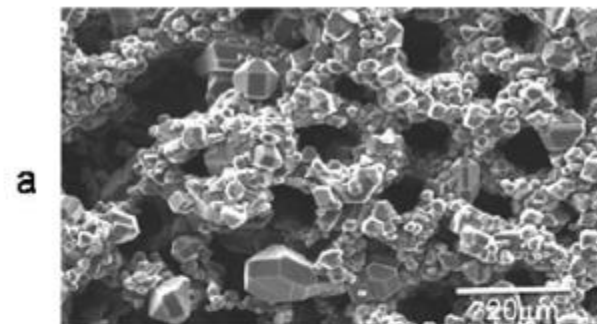
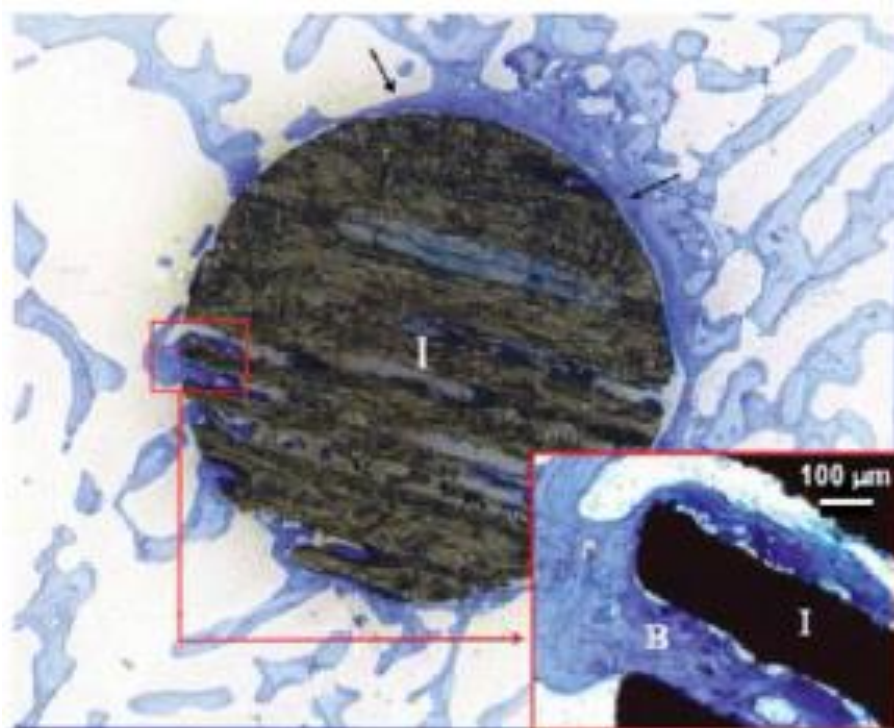
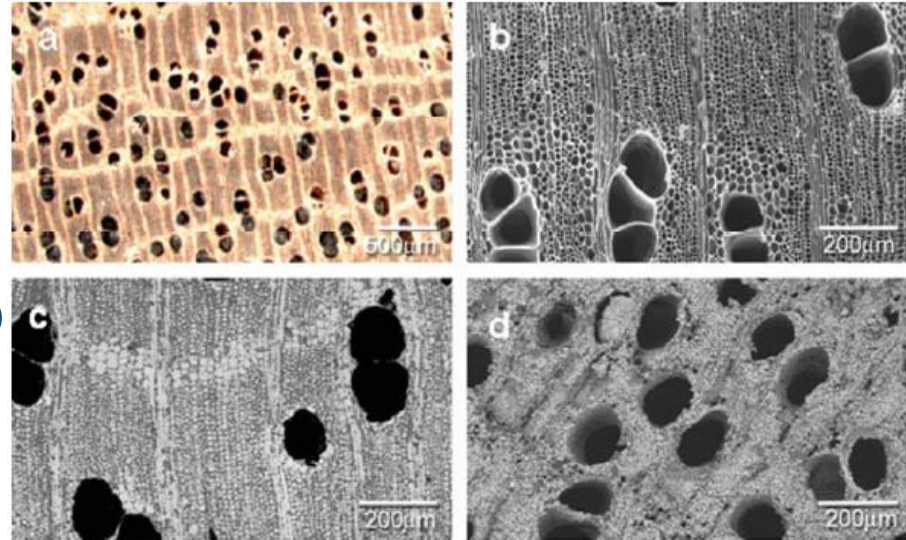
Hidroxiapatita (diente de tiburón)



Laboratorio investigación:

BIOMATERIALES

Carburo de silicio (maderas, pirolización)



ACTIVIDAD ASISTENCIAL:



Veterinary Quarterly, 2014
<http://dx.doi.org/10.1080/01652176.2014.993094>



CASE REPORT

Intracranial epidural empyema due to *Cryptococcus neoformans* in a 5-year-old neutered male European short hair cat

L. Espino*, J. D. Barreiro, A. Gonzalez, G. Santamarina, N. Miño and S. Vazquez

Departamento de Ciencias Clínicas Veterinarias, Facultad de Veterinaria de Lugo, Universidad de Santiago de Compostela, Estrada da Granza s/n. 27702 Lugo, Spain

(Received 22 May 2014; accepted 25 November 2014)

Keywords: cat; computed tomography; *Cryptococcus*; epidural empyema; intracranial infection

Efusiones pleurales en pequeños animales

Pleural effusions in small animals

M. Suárez, A. González-Martínez, M. Vila, A. González-Cantalapiedra, G. Santamarina
Departamento de Ciencias Clínicas Veterinarias. Hospital Veterinario Universitario Rof Codina. Facultad de Veterinaria. Universidad de Santiago de Compostela

Resumen

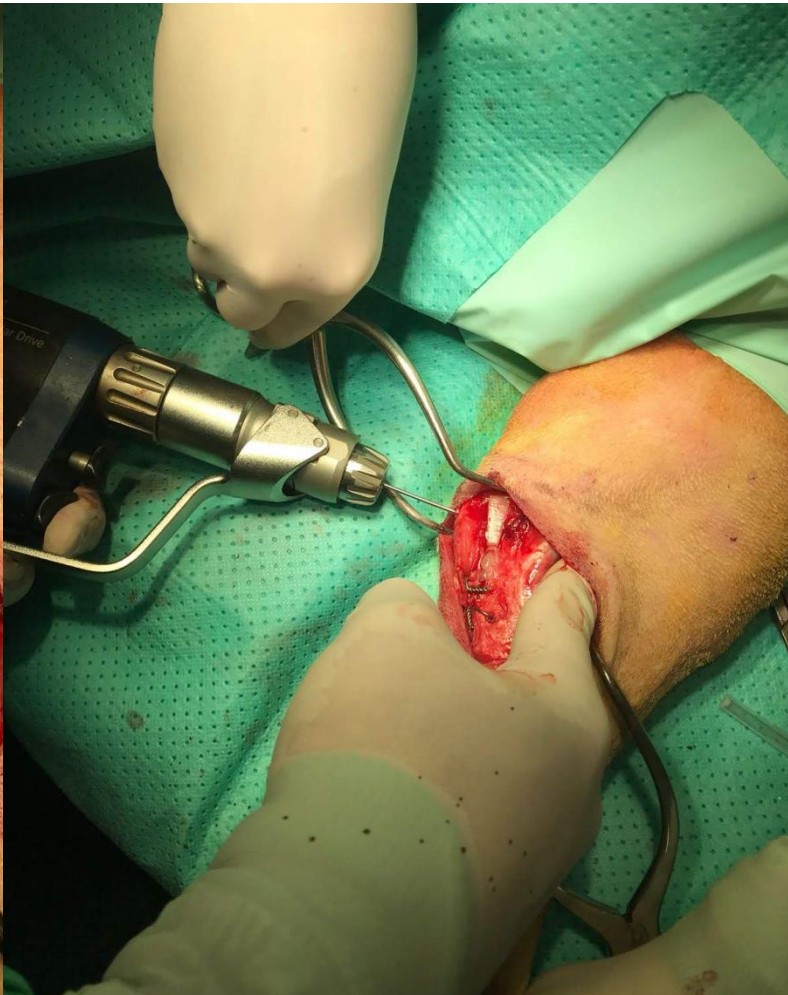
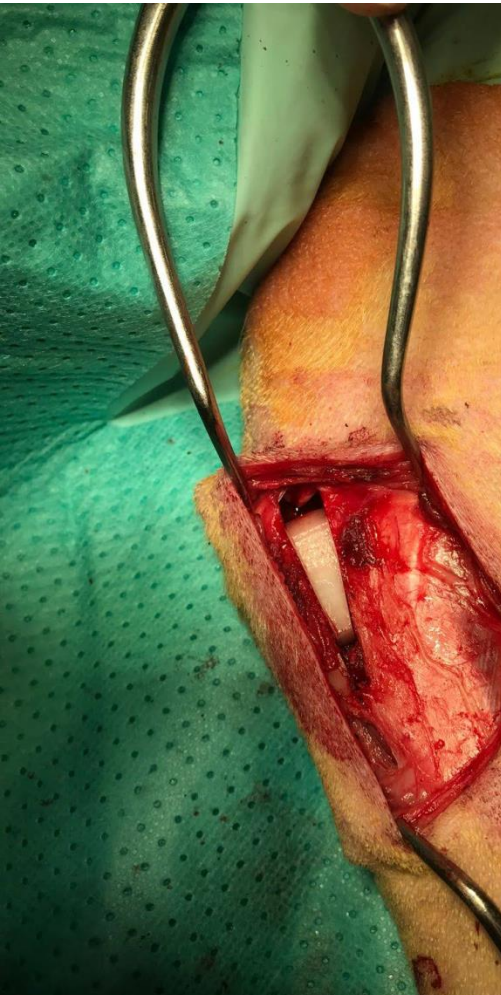
El derrame pleural es una acumulación anormal de líquidos en la cavidad pleural y constituye una manifestación clínica común a numerosos procesos. El derrame pleural es relativamente frecuente en perros y gatos. Su presentación clínica es variable, depende de la enfermedad subyacente, del volumen del derrame y de la rapidez en su formación. En ocasiones puede ser asintomático e identificarse como un hallazgo accidental, mientras que en otras es de tal magnitud que los signos de dificultad respiratoria dominarán el cuadro clínico. El planteamiento diagnóstico dependerá de las causas probables establecidas en función de la anamnesis y la exploración física de cada paciente en particular. La evaluación de un paciente con derrame pleural de causa no conocida comienza con la toracocentesis diagnóstica, excepto cuando la sospecha de derrame pleural es claramente secundaria a una enfermedad específica. El análisis del líquido pleural genera una información vital para el proceso diagnóstico, y en ciertos casos, suficiente para determinar la causa. El tratamiento es muy variable pues depende de la etiología subyacente. En ocasiones la causa puede no ser manejable. Los derrames neoplásicos generalmente tienen mal pronóstico y el tratamiento suele ser paliativo. Los pitorax tienen un pronóstico bueno, pero requieren de tratamiento con antibióticos riguroso y prolongado, y frecuentemente quirúrgico. Los trasudados, y derrames hemorrágicos son generalmente fáciles de resolver, pero las expectativas a largo plazo dependerán de la causa primaria. Los derrames quilosos pueden responder a tratamiento dietético y drenaje, pero si estos métodos fallan, será necesario realizar tratamiento quirúrgico.



Palabras clave: Líquido pleural, Efusión pleural, Pitorax, Quilotorax, Hemotorax.
Keywords: Pleural fluid, Pleural effusion, Pyothorax, Chylothorax, Hemothorax.
Clin. Vet. Peq. Anim., 2012, 32 (2): 65-78

ACTIVIDAD ASISTENCIAL:

Diseño de un nuevo implante para realizar el avance de la tuberosidad tibial (TTA), patente solicitada.



GRACIAS